


## Ghost surface polariton in antiferromagnets

Haoyuan Song<sup>1</sup>, Xiangguang Wang, Yuqi Zhang, Shaopeng Hao, and Xuan-Zhang Wang<sup>\*</sup>  
 Key Laboratory for Photonic and Electronic Bandgap Materials, Chinese Ministry of Education,  
 and School of Physics and Electronic Engineering, Harbin Normal University, Harbin 150025, China

 (Received 9 October 2021; revised 9 July 2022; accepted 12 July 2022; published 28 July 2022)

A surface polariton was predicted in antiferromagnets in a simple geometry. It exhibits interesting characteristics. Its electromagnetic fields and energy-flux density both oscillate and attenuate with the distance from the surface. It is a ghost surface polariton (GSP) and is a magnetic-field-tunable surface polariton. The branch-interference produces a series of rapidly attenuated fringes. It exists only in an external magnetic field along the easy axis. The attenuated total reflection spectra obtained in the Otto configuration accurately demonstrate this GSP and show its excitation or observation path.

DOI: [10.1103/PhysRevB.106.024425](https://doi.org/10.1103/PhysRevB.106.024425)

### I. INTRODUCTION

Some magnetic materials or magnetic metamaterials were demonstrated to be a kind of hyperbolic material in specific situations [1–5]. In the case of no external magnetic field, the principal components of the permeability tensor in an insulative antiferromagnet (AFM) have opposite signs in the reststrahlen frequency band, so the dispersion equation is hyperbolic in this material. This hyperbolicity is supported by its permeability tensor rather than its permittivity (a positive scalar quantity), and is different from that of hBN and MoO<sub>3</sub> [6,7]. Naturally insulative AFMs form a large family including transition metal oxides, fluorides, and sulfides (e.g., NiO, MnO, FeF<sub>2</sub>, and MnF<sub>2</sub>) [8–10]. Due to their hyperbolicity, they have been attracting the attention of physicists again [11–13]. Engineering surface magnon polaritons (SMPs) were investigated in an external magnetic field orthogonal to the AFM easy axis [11], where the effect of external field on the SMPs was focused on. The Goos-Hänchen shift of reflected light beam from the AFM surface was investigated [12] and hyperbolic dispersion and negative refraction of the AFMs were discussed [13]. Recently, we predicted Dyakonov surface magnons and magnon polaritons [14].

Surface polaritons possess a common feature, i.e., their electromagnetic fields exponentially decay with the distance away from the surface. A conventional surface polariton propagates along the surface and has a definite polarization, e.g., a SMP is of TE polarization in an antiferromagnet or ferromagnet [9,10,15–18], a surface phonon or plasmon polariton is of TM polarization in polar crystals [10], metals or graphene systems [19–20]. We should mention surface hybrid-polarization polaritons in anisotropic materials, for example the Dyakonov-like surface phonon and plasmon polaritons [21–23], and Dyakonov magnon polaritons [14]. The surface hybrid-polarization polaritons are composed of two branches in the materials, whose branches generally decay

out of sync with the distance from the surface. A ghost surface phonon polariton was predicted [24] and was observed in experiment [25] recently. Its mathematical expression is similar to the ghost waves (or nonuniform plane waves) in anisotropic transparent materials [26–28]. Its main feature is that its electromagnetic fields not only exponentially attenuate but also sinusoidally oscillate with distance from the surface.

### II. DISPERSION EQUATION AND SMP FIELDS

In this paper, we will report another ghost surface polariton supported by an insulative AFM in the simplest geometry. The geometry and coordinate system are shown in Fig. 1, where both the external magnetic field ( $H_0$ ) and AFM easy axis are vertical to the surface. The permeability tensor is a nondiagonal matrix, namely

$$\vec{\mu} = \mu_0 \begin{pmatrix} 1 & 0 & 0 \\ 0 & \mu_1 & i\mu_2 \\ 0 & -i\mu_2 & \mu_1 \end{pmatrix}, \quad (1)$$

where  $\mu_1 = 1 + \psi_+ + \psi_-$  and  $\mu_2 = \psi_+ - \psi_-$  with  $\psi_{\pm} = \omega_m \omega_a / [\omega_2 - (\omega \pm \omega_0 + i\tau)^2]$  with damping constant  $\tau$  [9,10]. We should remind the reader that the specific frequencies included in the formulas are defined with the AFM physical parameters. For the FeF<sub>2</sub> crystal, its sublattice magnetization  $4\pi M_0 = 7.04$  kG is converted to  $\omega_m = 0.74$  cm<sup>-1</sup>, exchange field  $H_e = 540.0$  kG to  $\omega_e = 56.44$  cm<sup>-1</sup>, and anisotropic field  $H_a = 200.0$  kG to  $\omega_a = 20.9$  cm<sup>-1</sup> [12,15]. The zero-field resonant frequency  $\omega_r = \{\omega_a(2\omega_e + \omega_a)\}^{1/2} \approx 52.877$  cm<sup>-1</sup> and  $\omega_0 = \gamma H_0$  and gyromagnetic ratio  $\gamma = 0.1045$  cm<sup>-1</sup>/kG. The AFM has two resonant frequencies linearly changing with  $H_0$ ,  $\omega_r - \omega_0$  and  $\omega_r + \omega_0$ . Its permittivity is  $\epsilon_a = 5.5$ . In order to be consistent with the experiments [10,17] and for convenience, all frequencies included in the above formulas have been divided by  $2\pi c$  ( $c$  is the vacuum light velocity), or these frequencies are reduced frequencies and their unit is cm<sup>-1</sup>. In the subsequent theoretical analysis and derivation, the wave-vector and

<sup>\*</sup>Corresponding author: xzwang696@126.com

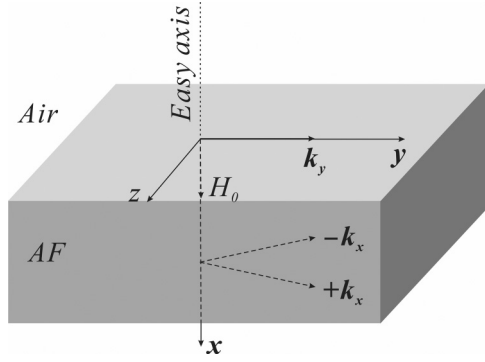


FIG. 1. Geometry and coordinate system used in theory, where both the AFM easy axis and external magnetic field are vertical to the surface and the surface polariton propagates along the  $y$  axis. The  $y$ - $z$  plane is the surface or the air-AFM interface. Two dashed arrows with  $\pm k_x$  indicate the propagating directions of two branches in the AFM.

attenuating constants will be divided by  $2\pi c$  and have the same unit as that of frequency  $\omega$ .

For convenience, we ignore the damping term and assume that a surface magnon polariton propagates along the  $y$  axis and its fields attenuate with the distance away from the surface. Leaving out the common factor  $\exp[2\pi i(k_y y - c\omega t)]$  in the expressions of SMP fields, the magnetic field is written as  $\mathbf{H}' \exp(2\pi \Gamma' x)$  with attenuating constant  $\Gamma' = (k_y^2 - \omega^2)^{1/2}$  above the AFM. We use  $\mathbf{H} \exp(-2\pi \Gamma x)$  to express the magnetic field in the AFM, where  $\Gamma$  is a formal attenuation constant whose real part is the actual attenuation constant and the imaginary part is the oscillating constant and meanwhile  $k_y$  is the wave vector.  $\mathbf{H}$  and  $\mathbf{H}'$  are the field amplitudes at the surface and  $\mathbf{H}$  fulfils the following equations:

$$(k_y^2 - \varepsilon_a \omega^2) H_x - ik_y \Gamma H_y = 0, \quad (2a)$$

$$-ik_y \Gamma H_x - (\Gamma^2 + \varepsilon_a \mu_1 \omega^2) H_y - i\varepsilon_a \mu_2 \omega^2 H_z = 0, \quad (2b)$$

$$i\varepsilon_a \mu_2 \omega^2 H_y + (k_y^2 - \Gamma^2 - \varepsilon_a \mu_1 \omega^2) H_z = 0. \quad (2c)$$

By the conventional method [9,10] as shown in Supplemental Material 1 [29], we find two solutions of  $\Gamma$  to satisfy

$$\Gamma_{\pm}^2 = [-b \pm (b^2 - 4c')^{1/2}]/2, \quad (3a)$$

with

$$b = \mu_1(\varepsilon_a \omega^2 - k_y^2) + (\varepsilon_a \mu_1 \omega^2 - k_y^2), \quad (3b)$$

$$c' = \mu_1(\varepsilon_a \mu_1 \omega^2 - k_y^2)(\varepsilon_a \omega^2 - k_y^2) + \varepsilon_a(\mu_2 \omega)^2(k_y^2 - \varepsilon_a \omega^2). \quad (3c)$$

We define the discriminant  $D = b^2 - 4c'$  for convenience and it is specifically written as

$$D = [\mu_1(\varepsilon_a \omega^2 - k_y^2) - (\varepsilon_a \mu_1 \omega^2 - k_y^2)]^2 - 4\varepsilon_a(\mu_2 \omega)^2(k_y^2 - \varepsilon_a \omega^2). \quad (4)$$

For  $H_0 = 0$ ,  $\mu_2 = 0$  so that  $D > 0$ . In this case, applying the boundary condition of electromagnetic fields, we easily

find one conventional SMP with TE polarization, which satisfies  $\mu_1 \Gamma' + \Gamma = 0$  with  $\Gamma = \sqrt{\mu_1(k_y^2 - \varepsilon_a \omega^2)}$  and it exists in the region of  $\mu_1 < 0$  and  $k_y < \sqrt{\varepsilon_a} \omega$ . Its dispersion curve is a curve segment in the  $\omega$ - $k_y$  space. To the best of our knowledge, we have not found any research that specifically discusses surface magnon polaritons at the antiferromagnetic surface in this geometry and case.

For  $H_0 \neq 0$ ,  $\mu_2 \neq 0$  and then the three components of magnetic field couple with together in the AFM. If there is any SMP, it is neither a TE wave nor a TM wave, but it is a hybrid-polarization surface wave. It is useful to discuss two cases according to the discriminant value. In the first case,  $D > 0$ , a SMP is found in the  $k_y$  range similar to that range where the zero-field SMP appears. It is an ordinary hybrid-polarization surface wave. In the second case,  $D < 0$ , we will find a unique SMP. Subsequently, we discuss and analyze only this unique SMP in the second case. Because the first term of  $D$  is certainly a positive value,  $k_y$  in the second term of  $D$  must be large enough to guarantee  $D < 0$ . It proves that the unique SMP exists in the range of large  $k_y$ . In addition,  $D > 0$  in the limit of large  $k_y$ , so the dispersion curve of the unique SMP is only a finite curve. It is obvious that  $\Gamma_{\pm}^2$  certainly is two complex quantities in this case, so  $\Gamma_{\pm}$  have four complex solutions. We can select only two solutions with  $Re(\Gamma_{\pm}) > 0$  for the SMP. Therefore, we achieve from Eq. (3a) that [29]

$$\Gamma_+ = \alpha + ik_x, \quad \Gamma_- = \alpha - ik_x, \quad (5)$$

which indicates that the SMP consists of two branches in the AFM and is of hybrid polarization. The two branches have the same attenuating constant

$$\alpha = [a' + (a'^2 + b'^2)^{1/2}]^{1/2}/\sqrt{2}, \quad (6a)$$

and opposite-sign oscillating constants or  $\pm k_x$ ,

$$k_x = [-a' + (a'^2 + b'^2)^{1/2}]^{1/2}/\sqrt{2}, \quad (6b)$$

where  $a'$  is the real part and  $b'$  is the imaginary part of  $\Gamma_{\pm}^2$ . It is evident that they are real quantities. Therefore, the two branches have the same attenuating constant  $\alpha$  but have different wave vectors,  $(-k_x, k_y)$  and  $(+k_x, k_y)$ . Thus, we use  $\mathbf{h} = \mathbf{H}^+ \exp(-2\pi \Gamma_+ x) + \mathbf{H}^- \exp(-2\pi \Gamma_- x)$  to express the SMP magnetic-field in the AFM, where  $\mathbf{H}^{\pm}$  are the amplitude vectors of the branch fields at the surface. The field components of either branch couple together in the response frequency range, so the other components can be expressed as functions of the  $y$  component. Using Eqs. (2a) and (2c) we have  $H_x^{\pm} = i\lambda_{\pm} H_y^{\pm}$  and  $H_z^{\pm} = i\eta_{\pm} H_y^{\pm}$  with

$$\lambda_{\pm} = k_y \Gamma_{\pm} / (k_y^2 - \varepsilon_a \omega^2), \quad (7a)$$

$$\eta_{\pm} = \varepsilon_a \mu_2 \omega^2 / (\varepsilon_a \mu_1 \omega^2 - k_y^2 + \Gamma_{\pm}^2), \quad (7b)$$

where  $\Gamma_+^* = \Gamma_-$ ,  $\lambda_+^* = \lambda_-$  and  $\eta_+^* = \eta_-$ . The electric-field tangential components of either branch are necessary for one to solve the dispersion relation of SMP, so according to  $\mathbf{e} =$

$i\nabla \times \mathbf{h} / \varepsilon_0 \varepsilon_a \omega$  and introducing  $\delta = \frac{\sqrt{\mu_0}}{\varepsilon_0 \varepsilon_a \omega}$  for convenience, the electric amplitudes at the surface are achieved to be

$$\begin{aligned} E_y^{\pm} &= -\delta \Gamma_{\pm} \eta_{\pm} H_y^{\pm}, \\ E_z^{\pm} &= i\delta (k_y \lambda_{\pm} - \Gamma_{\pm}) H_y^{\pm}, \end{aligned} \quad (8)$$

which also indicate the relations between the electric and magnetic fields, and meanwhile the electric-field tangential amplitudes of SMP are  $E_y^+ + E_y^-$  and  $E_z^+ + E_z^-$ . The electromagnetic boundary conditions at the surface lead to dispersion equation [30]

$$\text{Im}\{\eta(\varepsilon_a\Gamma' + \Gamma)[\varepsilon_a\omega^2 + \Gamma'(k_y\lambda^* - \Gamma^*)]\} = 0, \quad (9)$$

with  $\Gamma = \Gamma_+$ ,  $\lambda = \lambda_+$  and  $\eta = \eta_+$ . We will readily find a surface-polariton solution from the above dispersion equation.

In order to discuss the electromagnetic fields of SMP in the AFM, we assume that  $H_y^- = \Lambda H_y^+$ . From the continuity of  $h_z$  and  $e_y$  at the antiferromagnet-air interface, we find that  $\Lambda = -\eta(\varepsilon_a\Gamma' + \Gamma)/\eta^*(\varepsilon_a\Gamma' + \Gamma^*)$  with  $\Lambda\Lambda^* = 1$  and  $[\Lambda/(1 + \Lambda)]^* = 1/(1 + \Lambda)$ . We easily prove  $|H_y^+| = |H_y^-|$ ,  $|H_x^+| = |H_x^-|$  and  $|H_z^+| = |H_z^-|$ , and find similar relations between the branch electric fields. It means that the two corresponding branch-field components have the same field amplitude but have different phases. It completely differs from the existing surface hybrid-polarization polaritons [14,21–23], where there are different amplitudes but the same phase. The superposition of the branch magnetic fields produces the SMP magnetic field [31] to be

$$h_y = 2H'_y e^{-2\pi\alpha x} [R_y \cos(2\pi k_x x) + I_y \sin(2\pi k_x x)], \quad (10a)$$

where  $R_y$  and  $I_y$  are the real and imaginary parts of  $1/(1 + \Lambda)$ , and

$$h_{x,z} = 2iH'_y e^{-2\pi\alpha x} [R_{x,z} \cos(2\pi k_x x) + I_{x,z} \sin(2\pi k_x x)], \quad (10b)$$

where  $R_x$  and  $I_x$  are the real and imaginary parts of  $\lambda/(1 + \Lambda)$ , but  $R_z$  and  $I_z$  are the real and imaginary parts of  $\eta/(1 + \Lambda)$ .  $H'_y$  is the magnetic-amplitude component on the surface. Due to the relation  $\mathbf{e} = i\delta\nabla \times \mathbf{h}$ , the electric field is easy to be obtained,

$$\mathbf{e} = \delta \left[ -k_y h_z, -i \frac{\partial h_z}{\partial x}, i \left( \frac{\partial h_y}{\partial x} - ik_y h_x \right) \right]. \quad (11)$$

The phase difference between  $h_y$  and  $h_x$  or  $h_z$  is equal to  $\pm\pi/2$  and that between  $e_y$  and  $e_x$  or  $e_z$  also is  $\pm\pi/2$ . The

phase relations between the electric and magnetic fields also are very simple. The SMP moves along the y axis. We realize that the main features of the SMP as follows. (i) Its two branch fields have the same amplitude but have different phases, which leads to their interference in the AFM. (ii) There are very simple phase relations among its electromagnetic-field components. (iii) The SMP moves along the y axis (or along the surface) and its electromagnetic fields oscillates and attenuates with the distance from the surface. The SMP is a ghost surface polariton (GSP) propagating along the surface plane. (iv) no GSP exists when there is no external magnetic field. The external magnetic field is a necessary condition for the existence of GSP.

In contrast to the previous GSP [24,25], this GSP is a hybrid-polarization wave composed of the two branches and its field-oscillating factors are real functions of  $k_x x$ . It is the most interesting that the GSP intensity will exhibit interferent fringes on the plane normal to the propagation direction in the AFM. It should be noted that the previous GSP actually

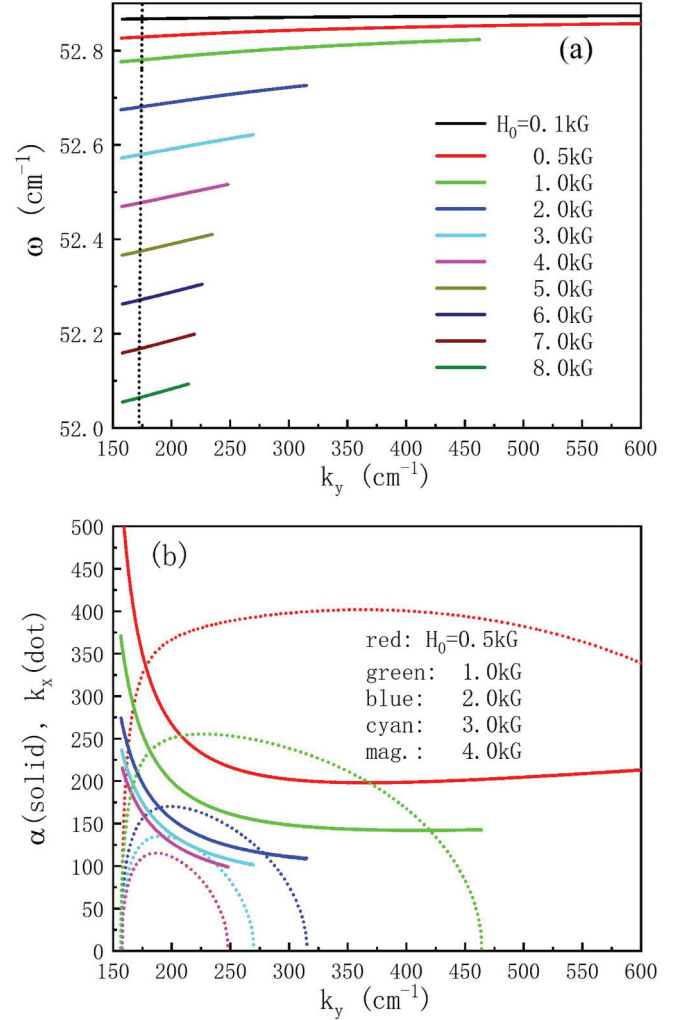


FIG. 2. (a) Dispersion curves of the GSP for various values of  $H_0$ , where the dot line is the scanning line of ATR numerical simulation with incident angle  $\theta = 45^\circ$  and prism permittivity 21.9 (CdO). (b) The attenuating and oscillating constants as functions of wave number, where the solid curves show  $\alpha$  and the dotted curves represent  $k_x$ .  $k_x$  and  $\alpha$  have the same unit as  $k_y$ .

propagates in the x-y plane and the corresponding oscillating factor is  $\exp(ik_x x)$  [24,25].

### III. NUMERICAL CALCULATIONS

Numerical calculations are based on antiferromagnetic FeF<sub>2</sub> with the physical parameters given previously. Figure 2(a) illustrates dispersion curves of the GSP. We see that the GSP is situated in the region of  $\omega < \omega_r = 52.877 \text{ cm}^{-1}$  and  $k > 150 \text{ cm}^{-1}$ . The GSP is a magnetic-field-tunable SMP and its dispersion curve is a finite curve segment, as described in Fig. 2(a). Attenuating constant  $\alpha$  and oscillating constant  $k_x$  are very important to characterize the GSP.  $\alpha$  shows the localization at the surface and  $k_x$  reflects the oscillating behavior. Figure 2(b) shows the two constants. The oscillating phenomenon is obviously visible only if  $k_x$  is larger than  $\alpha$ , so this phenomenon is weaker for a larger value of  $H_0$ . Figure 2(b) also reflects that the left and right endpoints of

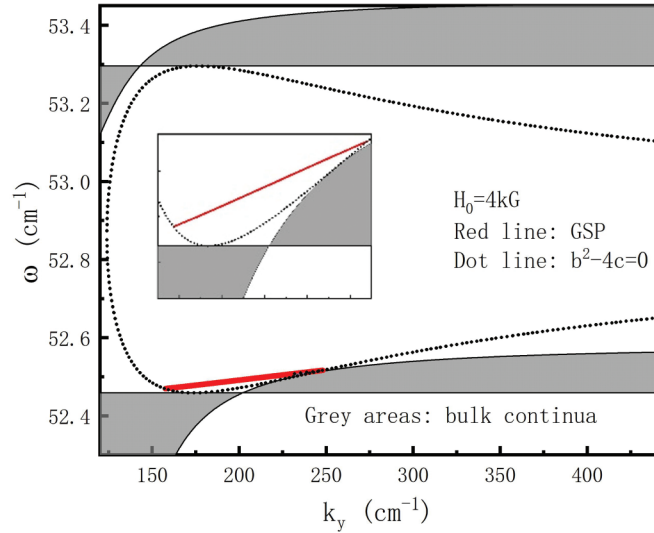


FIG. 3. Polariton-spectrum structure for  $H_0 = 4$  kG. The dotted line is obtained from  $b^2 - 4c = 0$  and the red solid line represents the GSP. The bulk modes occupy the grey areas or bulk continua. The inset enlarges the vicinity of the GSP dispersion curve.

each dispersion curve in Fig. 2(a) both correspond to  $k_x = 0$ , where  $D = 0$  and the oscillating effect disappears.

In order to examine the polariton-spectrum structure in the present geometry, we offer Fig. 3 for  $H_0 = 4$  kG as an example. The GSP exists only in the region surrounded by the dotted curve obtained from  $D = 0$ . Bulk polaritons move in the  $x$ - $y$  plane and form bulk continua as shown by the grey areas. The horizontal boundaries of the grey areas correspond to the two resonant frequencies of the AFM, respectively. We see that the GSP dispersion curve starts from a point and terminates at another point on the dotted curve.

It is clearly seen from the inset that the GSP and bulk continua are completely separated by the dotted curve. Figure 3 partially shows the spectrum-structure diagram including the GSP. The rest contains only bulk continua and can be imagined [10,16].

Figure 4(a) illustrates the distribution of magnetic field in the AFM. We see the evident attenuating-oscillating effect, where  $\alpha$  is obviously smaller than  $k_x$ . At the surface, the  $x$  and  $y$  components are much larger than the  $z$  component, so a TE incident radiation is more suitable in the Otto configuration for one to excite and observe the GSP. The energy-flux density [ $S = \text{Re}(\mathbf{e}^* \times \mathbf{h})/2$ ] represents both the GSP intensity and energy transmission. Expressions (10) and (11) imply that  $\mathbf{S}$  is along the  $y$  axis. Figure 4(b) shows the energy-flux-density distribution in the AFM. The attenuating-oscillating effect also is obviously reflected.  $\mathbf{S}$  is either parallel or antiparallel to the  $y$  axis, dependent on  $x$ . Thus, the radiation intensity of the GSP exhibits a series of interferent fringes on the plane normal to the  $y$  axis and its maximum is situated inside the AFM, not lying on the surface. These phenomena come from the interference of the two branches.

$H_0$  is important for the existence and dispersion properties of the GSP. The inversion of  $H_0$  leads to that  $\eta$ ,  $h_z$ ,  $e_x$ , and  $e_y$  change in sign, so the polarization feature is changed. Despite this, the dispersion equation and energy-flux density both are

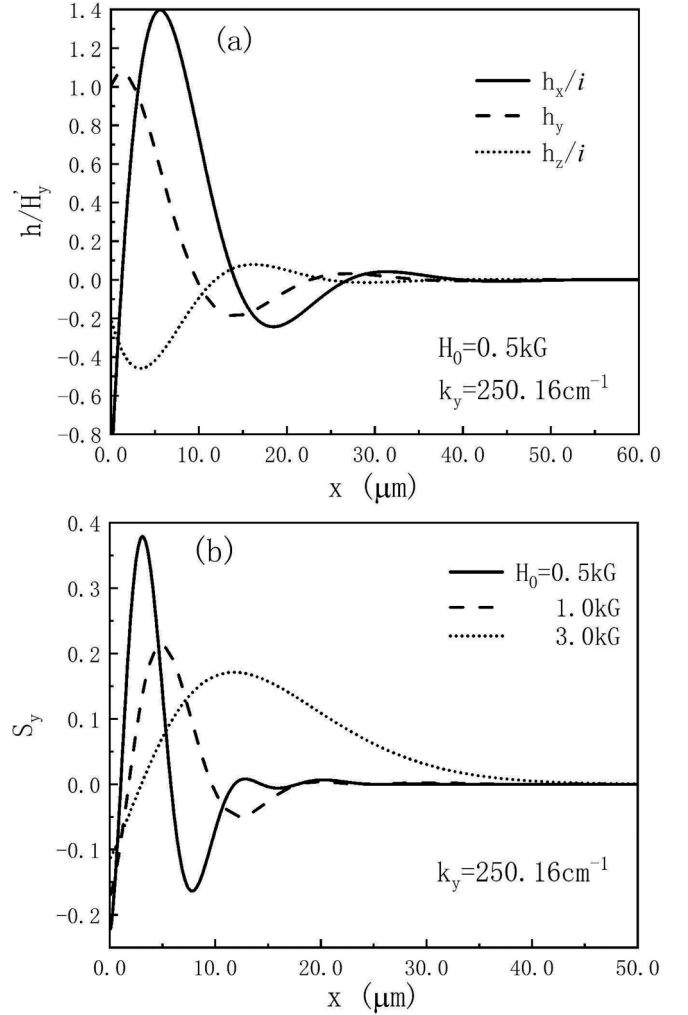


FIG. 4. (a) The magnetic-field distribution of GSP in the AFM for  $H_0 = 0.5$  kG and  $k_y = 250.16$   $\text{cm}^{-1}$ , where  $i$  in the legend indicates the phase difference between  $H_y$  and  $H_{x,z}$ . (b) The distribution of energy-flux density in the AFM for various values of  $H_0$ , where  $\mathbf{S}$  has only the  $y$  component and is measured in  $\delta f |H_y|^2$ .

unchanged, different from those of conventional SMPs in the Voigt geometry [9,10]. The difference originates from the easy axis or  $H_0$  normal to the surface in our geometry. For the previous GSP [24,25], the energy-flux density monotonously decays with  $x$ , so there are not oscillating behavior and interferent fringes. Therefore, this new GSP is more interesting.

According to the standard numerical simulating method [32] of attenuated total reflection (ATR) in the Otto geometry [10,14,17], we obtain the ATR spectra for a TE incident radiation, where the incident angle is fixed at  $45^\circ$  and the CdO prism with dielectric constant  $\epsilon_p = 21.9$  [33] is applied. The gap width is  $10$   $\mu\text{m}$  between the AFM and prism. Figure 5 illustrates the ATR spectra along the scanning line in Fig. 2(a). It is found that the sharp dips of ATR curves accurately correspond to the intersections of the dispersion curves and scanning line in Fig. 2(a), respectively. It further demonstrates that the solution of dispersion Eq. (9) represents an actual GSP. For  $H_0 = 1$  kG, besides the sharp dip, the green curve shows another evident decrease about  $\omega = 53$   $\text{cm}^{-1}$ . The de-



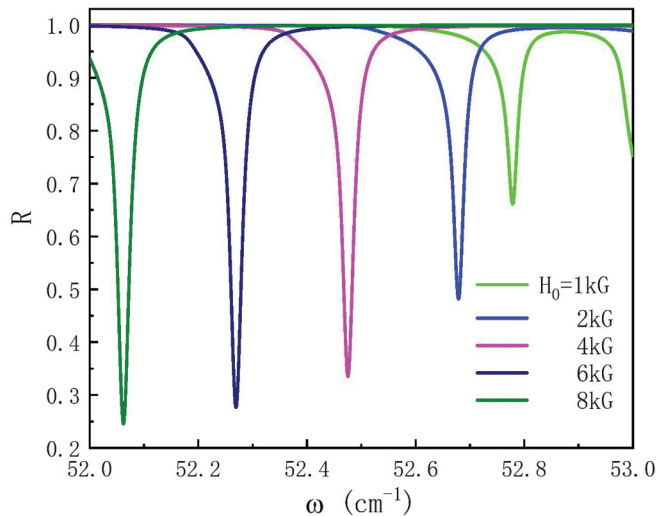


FIG. 5. ATR spectra in the Otto configuration for various values of external magnetic field, where the TE incidence is used and the incident angle is  $45^\circ$ . The gap thickness is  $10 \mu\text{m}$  and the dielectric constant of the CdO prism is equal to 21.9 [29]. We take the damping constant  $\tau = 0.01$  and  $R$  is the reflective ratio.

crease is related to the bulk continuum like the upper-right bulk continuum illustrated in Fig. 3 for  $H_0 = 4 \text{ kG}$ . For the other external fields, the similar picture also can be found outside the figure window. The excitation of bulk polaritons is closely related to the polarization of incidence. Bulk-polariton excitation is very weak in the figure window for the TE incidence. In addition, we found that the dips related to the GSP are small and blunt but bulk polaritons are remarkably excited for a TM incident radiation in the same circumstance, especially in the figure window. Therefore, the GSP is more easily excited and observed with TE incident radiations.

#### IV. CONCLUSIONS

In the simplest configuration shown by Fig. 1, no surface magnon polariton has been found in the past. However, one GSP has been predicted here. It is composed of two branches in the AFM, which have the same attenuation amplitude, but possess different phases. Its electromagnetic fields oscillate and attenuate with the distance ( $x$ ) from the surface. The main differences from the previous ghost surface polariton are (i) it is composed of two coherent branches and propagates along the surface plane (the  $y$  axis), the maximum of its radiation is situated inside the AFM, and (ii) its energy-flux density exhibits the oscillating-attenuating behavior and forms inter-ferent fringes on the plane normal to its propagation direction. (iii) its energy flux is either parallel or antiparallel to its propagation direction, dependent on  $x$ . The GSP is  $H_0$  tunable and  $H_0$  is its necessary condition of existence. These features are very unique. At the surface, it is more like a TE wave, so a TE incident radiation easily excites this GSP in the Otto configuration. The ATR spectra further clearly prove the existence of the GSP and point out the path of its excitation or observation.

In physics, the GSP fundamentally originates from the gyromagnetic permeability tensor of the AFM, especially its nondiagonal elements. Due to the permeability tensor of ferromagnetic and ferrimagnetic materials similar to that of the AFM, they also can support this style of GSP. In addition, optically active media and plasmonic materials in an external magnetic field possess a similar permittivity tensor [10], so one may find similar GSP in them. The interesting properties of this GSP imply the possibility of surface-polariton applications.

#### ACKNOWLEDGMENTS

This work was financially supported by Natural Science Foundation of Heilongjiang Province with ZD2009103. The authors declare no conflicts of interest.

- [1] S. S. Kruk, Z. J. Wong, E. Pshenay-Severin, K. O'Brien, D. N. Neshev, Y. S. Kivshar, and X. Zhang, Magnetic hyperbolic optical metamaterials, *Nat. Commun.* **7**, 11329 (2016).
- [2] R. Macêdo, K. L. Livesey, and R. E. Camley, Using magnetic hyperbolic metamaterials as high frequency tunable filters, *Appl. Phys. Lett.* **113**, 121104 (2018).
- [3] J. Song, L. Lu, Q. Cheng, and Z. Luo, Three-body heat transfer between anisotropic magneto-dielectric hyperbolic metamaterials, *J. Heat Transfer* **140**, 082005 (2018).
- [4] R. Pomezov, I. A. Kolmychek, E. A. Gan'shina, O. Y. Volkova, A. P. Leont'ev, K. S. Napol'skii, and T. V. Murzina, Optical effects in magnetic hyperbolic metamaterials, *Phys. Solid State* **60**, 2264 (2018).
- [5] Y. Wang, Z. Guo, Y. Chen, X. Chen, H. Jiang, and Hong Chen, Circuit-based magnetic hyperbolic cavities, *Phys. Rev. Applied* **13**, 044024 (2020).
- [6] S. Dai, Z. Fei, Q. Ma, A. S. Rodin, M. Wagner, A. S. McLeod, M. K. Liu, W. Gannett, W. Regan, K. Watanabe, T. Taniguchi, M. Thiemens, G. Dominguez, A. H. Castro Neto, A. Zettl, F. Keilmann, P. Jarillo-Herrero, M. M. Fogler, and D. N. Basov, Tunable phonon polaritons in atomically thin van der Waals crystals of boron nitride, *Science* **343**, 1125 (2014).
- [7] M. N. Gjerding, R. Petersen, T. G. Pedersen, N. A. Mortensen, and K. S. Thygesen, Layered van der waals crystal with hyperbolic light dispersion, *Nat. Commun.* **8**, 320 (2017).
- [8] S. V. Vonsovskii, *Magnetism*, Vol. 2 (Keter Publishing House, Jerusalem, 1974), Chap. 22.
- [9] K. Abraha and D. R. Tilley, Theory of far infrared properties of magnetic surfaces, films and superlattices, *Surf. Sci. Rep.* **24**, 125 (1996).
- [10] M. G. Cottam and D. R. Tilley, *Introduction to Surface and Superlattice Excitations* (IOP Publishing Ltd, Philadelphia, 2005), Chaps. 2, 6, and 9.
- [11] R. Macêdo and R. E. Camley, Engineering terahertz surface magnon-polaritons in hyperbolic antiferro-magnets, *Phys. Rev. B* **99**, 014437 (2019).
- [12] V. B. Silva and T. Dumelow, Surface mode enhancement of the Goos-Hänchen shift in direct reflection off antiferromagnets, *Phys. Rev. B* **97**, 235158 (2018).

- [13] K. Grishunin, T. Huisman, G. Li, E. Mishina, T. Rasing, A. V. Kimel, K. Zhang, Z. Jin, S. Cao, W. Ren, G.-H. Ma, and R. V. Mikhaylovskiy, Terahertz magnon-polaritons in  $\text{TmFeO}_3$ , *ACS Photonics* **5**, 1375 (2018).
- [14] Shaopeng Hao, Shufang Fu, Sheng Zhou, and Xuan-Zhang Wang, Dyakonov magnons and magnon polaritons, *Phys. Rev. B* **104**, 045407(2021).
- [15] R. L. Stamps and R. E. Camley, Green's function for antiferromagnetic polaritons, I. Surface modes and resonances, *Phys. Rev. B* **40**, 596 (1989).
- [16] R. E. Camley and D. L. Mills, Surface-polaritons on uniaxial antiferromagnets, *Phys. Rev. B* **26**, 1280 (1982).
- [17] M. R. F. Jensen, T. J. Parker, K. Abraha, and D. R. Tilley, Experimental Observation of Surface Magnetic Polaritons in  $\text{FeF}_2$  by Attenuated Total Reflection (ATR), *Phys. Rev. Lett.* **75**, 3756 (1995).
- [18] Xuan-Zhang Wang and D. R. Tilley, Retarded modes of a lateral antiferromagnetic/nonmagnetic superlattice, *Phys. Rev. B* **52**, 13353 (1995).
- [19] S. Xiao, X. Zhu, B. H. Li, and N. A. Mortense, Graphene-plasmon polaritons: From fundamental properties to potential applications, *Front. Phys.* **11**, 117801 (2016).
- [20] S. Baher and Z. Lorestaniweiss, Propagation of surface plasmon polaritons in monolayer graphene surrounded by nonlinear dielectric media, *J. Appl. Phys.* **124**, 073103 (2018).
- [21] S. Fu, S. Zhou, Q. Zhang, and X.-Z. Wang, Completely confinement and extraordinary propagation of Dyakonov-like polaritons in hbn, *Opt. Laser Technol.* **125**, 106012 (2019).
- [22] C. J. Zapata-Rodríguez, J. J. Miret, S. Vuković, and M. R. Belić, Engineered surface waves in hyperbolic metamaterials, *Opt. Express* **21**, 19113 (2013).
- [23] E. Cojocaru, Comparative analysis of Dyakonov hybrid surface waves at dielectric–elliptic and dielectric–hyperbolic media interfaces, *J. Opt. Soc. Am. B* **31**, 2558 (2014).
- [24] S. Zhou, S. F. Fu, Q. Zhang, and X.-Z. Wang, Ghost surface phononic polaritons in ionic-crystal metamaterial, *J. Opt. Soc. Am. B* **35**, 2764 (2018).
- [25] W. Ma, G. Hu, D. Hu, R. Chen, T. Sun, X. Zhang, Q. Dai, Y. Zeng, A. Alu, C. Qiu, and P. Li, Ghost hyperbolic surface polaritons in bulk anisotropic crystals, *Nature (London)* **596**, 362 (2021).
- [26] T. G. Mackay and A. Lakhtakia, Exorcizing ghost waves, *Optik (Stuttg.)* **192**, 162926 (2019).
- [27] W. Iqbal, Q. A. Naqvi, and M. J. Mughal, Non-uniform plane waves (ghost waves) in general anisotropic medium, *Opt. Commun.* **453**, 124334 (2019).
- [28] E. Narimanov, Ghost resonance in anisotropic materials: Negative refractive index and evanescent field enhancement in lossless media, *Adv. Photon.* **1**, 4 (2019).
- [29] See Supplemental Material 1 at <http://link.aps.org/supplemental/10.1103/PhysRevB.106.024425> for the electromagnetic fields of surface magnon polariton.
- [30] See Supplemental Material 2 at <http://link.aps.org/supplemental/10.1103/PhysRevB.106.024425> for the dispersion relation.
- [31] See Supplemental Material 3 at <http://link.aps.org/supplemental/10.1103/PhysRevB.106.024425> for the specific electromagnetic fields and energy-flux density of GSP.
- [32] See Supplemental Material 4 at <http://link.aps.org/supplemental/10.1103/PhysRevB.106.024425> for the derivation of attenuated total reflection.
- [33] W. Paul, *Band Theory and Transport Properties (Handbook on SemiconductorS, Vol.1)* (North-Holland Publishing Company, Amsterdam, 1982), p.130.